Journal of Solar Energy Engineering

Technical Briefs

Performance of Chiller in a Solar Absorption Air Conditioning System With Partitioned Hot Water Storage Tank

Z. F. Li

K. Sumathy
e-mail: ksumathy@hkucc.hku.hk

Department of Mechanical Engineering, University of Hong Kong, Pokfulam Rd, Hong Kong

This paper reports the performance of a lithium bromide absorption chiller in a solar powered air conditioning system, when being operated conventionally. The chiller performance based on a modified solar powered absorption air conditioning system which is integrated with a partitioned storage tank has been presented and discussed. It is shown that, by partitioning the storage tank, the chiller performance is not significantly affected, and the solar powered cooling effect can be realized much earlier, achieving a higher total solar cooling COP_{system}, compared to the conventional system designs. [DOI: 10.1115/1.1345842]

1 Introduction

Currently, the most highly developed solar operated cooling equipment is the lithium bromide-water system which is readily available in commercial size [1,2]. The main components of a solar absorption cooling system are the absorption chiller, solar collector and hot water storage tank. In the present study, an attempt has been made to analyze the effect of partitioning the storage tank on the system's performance. In the morning, the collector system is connected to the upper part of the tank; and, in the afternoon, the whole tank is used to provide energy to the chiller. The purpose of the modification is to realize solar cooling effect as earlier as possible, and to achieve a higher total solar cooling COP_{system} compared to the conventional system designs (without any partition in the hot water storage tank).

2 System Description

Figure 1 shows the schematic diagram of a solar absorption air conditioning system comprising of four main flow circuits, taking into account of collector, generator, chilled water, and cooling water. As stated earlier, the storage tank is partitioned such that the upper part of the tank is connected to the collector in the morning and the whole tank is used in the afternoon to drive the chiller. As shown in Fig. 1, the partitioning of the storage tank is achieved by placing two baffle plates in the upper position of the tank, so that the tank is divided into two parts, with the upper part having one-fourth volume of the entire tank (partitioned mode). The basis for choosing the volume of the upper part has been described in detail in [3]. The two plates are perforated, so that while operating in the whole-tank mode, the collector returning flow in between the plates can locate at a position with the temperature close to its own. The criterion to choose the mode of operation depends on the temperature in the upper part of the tank. For the present absorption chiller, the minimum driving temperature is about 75°C, below which the performance declines sharply. Hence, when the upper part of the tank reaches above 75°C, the following criteria is checked, in order to connect the lower part of the storage tank and be treated as a whole-tank mode (lower + upper part):

$$Q_d \geqslant 0 \tag{1}$$

where Q_d is the difference of the useful solar energy gain (Q_U) and the cooling load (L_S). It is to be noted that, in the afternoon, even if $Q_d < 0$, the operation will continue in the whole-tank mode, as long as the water temperature in the lower part of the tank ($T_{S,2}$) is greater than 75°C.

3 Results and Discussion

A 4.7 kW solar powered air conditioning system designed and constructed by the staff and students of University of Hong Kong is located on the roof of Yam Pak building in HKU. A WFC-1.3 chiller manufactured by YAZAKI Company [4] with a rated capacity of 4.7 kW was tested in this study. The chiller has a generator inlet temperature range of 75-100°C, and a cooling water inlet temperature range of 24–31°C, and attains its rated capacity of 4.7 kW under the following conditions:

⇒Generator inlet temperature=88°C
⇒Cooling water inlet temperature=29.5°C
⇒Chilled water outlet temperature=9°C

The system employs a high-performance flat-plate collector of area 38 m^2, and a hot water storage tank of 2.75 m^3 in volume. In order to study the effect of partitioning, the storage tank is partitioned with an upper part having a volume of 1/4 of the entire tank. Experiments were carried out from 8:00 a.m. in the morning to 18:00 p.m. in the evening. For the early hours, as well as whenever the water temperature in the storage tank falls below the required threshold value (75°C), the auxiliary heater (set to the nominal value of 88°C) serves as the heat source to drive the chiller.

Figure 2 shows the inlet and outlet temperature profiles of source, cooling and chilled water during one-day operation. It can be seen that, early in the day, i.e. until 8:30 a.m., there is no cooling effect. Once the source temperature exceeds 80°C, the generator begins to operate. It should be mentioned here that, the initial required source temperature to generate water vapor is

Contributed by the Solar Energy Division of the American Society of Mechanical Engineers for publication in the JOURNAL OF SOLAR ENERGY ENGINEERING. Manuscript received by the ASME Solar Energy Division, Mar. 2000; final revision Nov. 2000. Associate Editor: G. Vliet

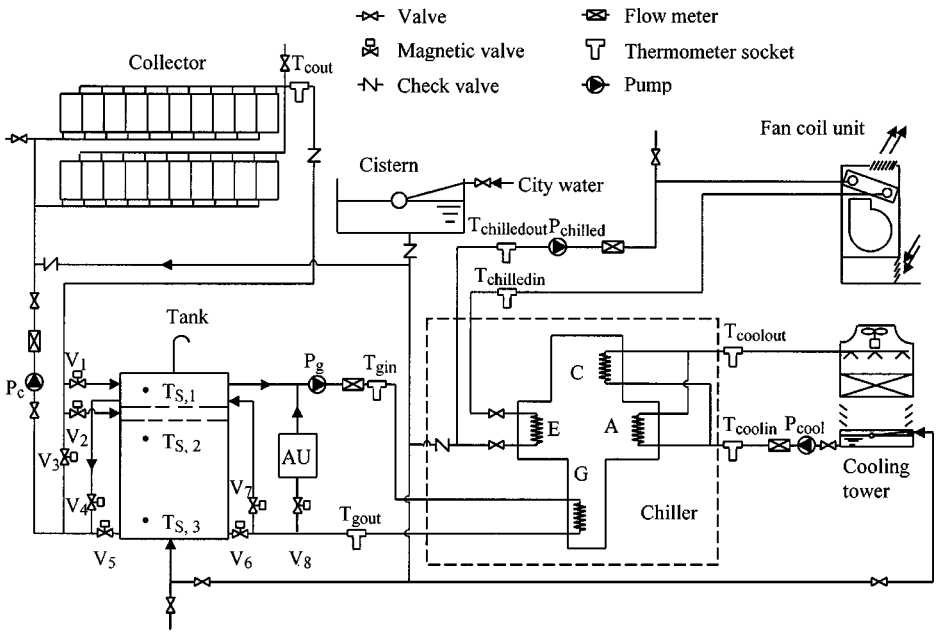

Fig. 1 Layout of the solar-powered absorption chiller

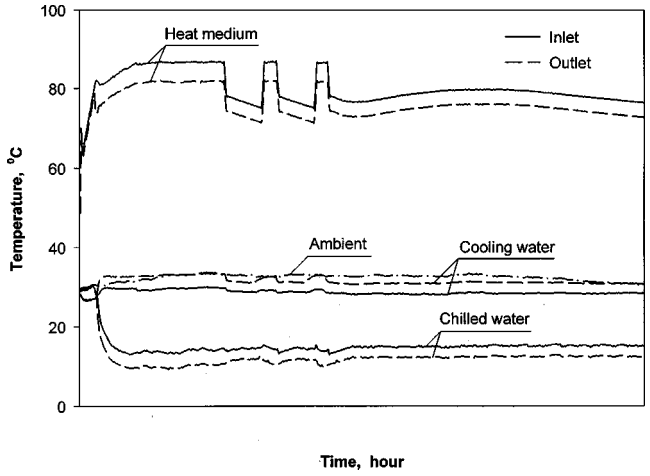

Fig. 2 Performance of chiller while operating on partitioned mode

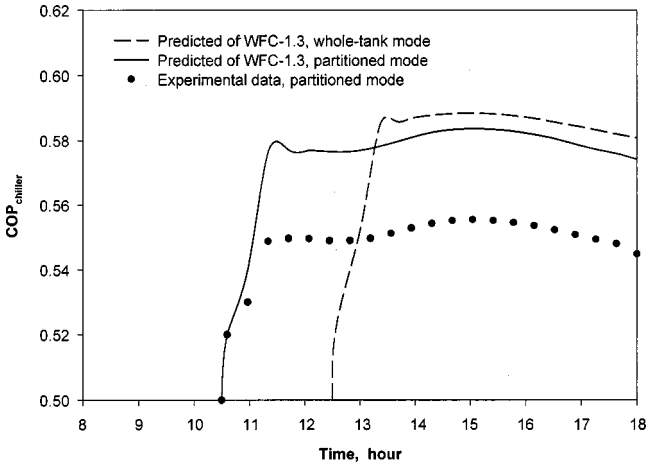

Fig. 3 Comparison of predicted instantaneous chiller $COP_{chiller}$ with experimental results of model WFC-1.3

higher than the required minimum driving temperature of about 75°C because of the existing temperature difference between the source and the generator. With time, the cooling water outlet temperature rises to a few degrees above ambient temperature, starting the ''cooling effect.'' At the same time, the chilled water outlet temperature gradually declines and finally attains a value of about 10°C. At 10:30 a.m., it can be seen that there is a sharp decrease in source temperature from 88°C to about 75°C, indicating that the chiller is now being connected to the storage tank and the auxiliary heater is switched off. Similar events occur between 11:45 to 12:45 hours, due to insufficient insolation. The water temperature in the storage tank is not high enough to drive the chiller, and occasionally the auxiliary heat is switched on to energize the chiller. At about 12:45 hours, the whole tank once again attains the required threshold temperature and the chiller produces cooling without any interruption, until 18:00 hours. It is also seen from Fig. 2 that, when the auxiliary heater is switched on (with an inlet temperature of about 88°C), the source inlet and outlet temperature difference is about 5.5°C, while when solar heat drives the chiller, the temperature difference is only about 4°C, and hence, the solar cooling effect is reduced.

Figure 3 compares the measured chiller $COP_{chiller}$ with the predicted values for the WFC-1.3 chiller during one day's operation, neglecting the influence of the auxiliary heater. In the morning the total cooling effect is produced by auxiliary heat, so the chiller $COP_{chiller}$ effected by solar energy is zero. As can be seen, for a partitioned mode, the system could provide solar cooling from about 10:30 hours, which is much earlier than for the conventional whole-tank mode (cooling effect is realized only from about 12:30 hours). Hence, the total solar cooling COP_{system} (the ratio of total cooling effect by solar energy to the total solar insolation) produced by partitioned mode is about 15% higher than for the whole-tank mode. This is mainly a result of the system being able to produce a cooling effect early in the day. Though the generating temperature in the partitioned mode is 1 to 2 degrees lower than in the whole-tank mode in the late afternoon, the $COP_{chiller}$ is not significantly affected. Therefore, for effective utilization of solar energy, a partitioned storage tank is strongly recommended. Also, it can be seen from the figure that, the experimental data for the WFC-1.3 deviates by only about 3–4% from the predicted

values. The deviation is mainly caused by the irreversibility of the processes, air leakage, and the inconsistent operating conditions due to the unsteady incident solar radiation.

4 Conclusion

A LiBr absorption chiller using partitioned storage has been analyzed. Experimental data are compared to the predicted values. It is shown that the partitioned mode system is more effective than the conventional system by about 15% in terms of the total solar cooling COP_{system}. Therefore, to realize earlier a solar coolingeffect and a higher COP_{system}, a partitioned storage tank is strongly recommended.

References

[1] Lamp, P., and Ziegler, F., 1998, ''European Research on Solar-Assisted Air Conditioning,'' Int. J. Refrig., **21**, pp. 89–99.
[2] Roberto, B., and Isaac, P., 1998, ''Solar Assisted Cooling with Sorption Systems: Status of the Research in Mexico and Latin America,'' Int. J. Refrig., **21**, pp. 100–115.
[3] Li, Z. F., and Sumathy, K., 1999, ''Performance of a Solar Absorption Air Conditioning System,'' *Third Int. Symp. on Heating, Ventilation, and Air Conditioning*, Shenzhen, China, Vol. 1, pp. 362–369.
[4] YAZAKI Company, 1975, *Installation and Serve Manual of YAZAKI Absorption Chiller*.

Thermal Model of an Absolute Solar Radiometer Designed for Future Satellite Missions

Y. J. Shen, D. H. Chen, and Z. M. Zhang*
Department of Mechanical Engineering,
University of Florida, Gainesville, FL 32611

This paper describes a finite-element thermal model of an absolute radiometer designed for total solar irradiance (TSI) measurement in future satellite missions. The cavity-type absolute radiometer employs the electrical-substitution technique and active temperature control to determine the radiant power entering the receiving cavity. The nonequivalence between the shutter-open mode and shutter-closed mode due to different temperature distributions is a major factor that affects the radiometric accuracy. The analysis shows that the nonequivalence is a function of sensor positions and can be minimized by properly choosing the electrical heating method and the temperature sensor location.

[DOI: 10.1115/1.1349551]

Introduction

Absolute radiometers using the electrical-substitution technique play an important role in the measurement of the total solar irradiance (TSI) and evaluation of the earth radiation budget [1,2]. The basic principle of electrical substitution is that equal electrical and radiant powers cause identical responses in the temperature sensor [3]. Prevailing radiometers are operated in the active mode where a temperature controller maintains the receiving cavity at a constant temperature (set point) by supplying electrical power before the shutter is opened. Once the shutter is opened, the incoming radiant power heats the cavity, and the temperature controller adjusts the electrical power to obtain the same temperature as the set point. The reduction in the electrical power is a measure of the radiant power.

*ASME member, corresponding author.

A series of satellite missions have been carried out to measure TSI from 1978 to 1997 [4]. Future satellite missions for the TSI measurement are needed for the reliable determination of the impact of solar radiation on the global climate change. More accurate radiometers with uncertainties of less than 0.1 percent are required to accomplish this kind of space-based measurement. Recently, new cavity-type absolute radiometers have been designed for future satellite missions [5]. These radiometers will be directly calibrated against the high-accuracy cryogenic radiometer [6] at the National Institute of Standards and Technology (NIST).

Thermal modeling and analysis are crucial to the evaluation and design of absolute radiometers [2,7]. This paper presents a thermal model using finite-element (FE) software, ANSYS 5.4 (ANSYS Inc., Canonsburg, PA), to assist in the evaluation of key issues of a proposed radiometer, including the responsivity, nonequivalence due to different heating methods, and the transient response including the time constant. The responsivity is the ratio of the steady-state temperature difference between the cavity (at the temperature sensor location) and the heat sink to the input power, and therefore it is proportional to the thermal resistance. For the radiometer design, the responsivity should be large enough to fulfill the resolution requirement. The nonequivalence between the electrical heating and radiant heating is the percentage difference of the steady-state temperature rises between the shutter-open and shutter-closed modes. The nonequivalence has always been a major concern for absolute radiometers since it directly affects the measurement uncertainty [3]. The time constant should be sufficiently small so that the steady-state condition can be achieved within a reasonable amount of time.

Figure 1 shows the absolute radiometer designed at NIST for TSI measurement with projected high accuracy, long-term stability, and robustness. The uniqueness of this design is that the long cavity itself acts as the thermal link between the heating region and the heat sink. The cavity is mounted on the heat sink at the opening. Silver is chosen as the cavity material to achieve a better temperature uniformity in the lower portion of the cavity and to reduce the radiative heat loss from the outside surface. The inner diameter of the cylinder is 10 mm. The wall thickness of the silver cavity is 100 μm from $Z=-5$ mm (the lowest point) to 10 mm, and 50 μm from $Z=10$ to 65 mm (the opening). The interior surface of the cavity is coated with 25-μm-thick nickel-phosphorus black. The end plate is slanted at 45° to achieve an effective absorption greater than 0.9999, with the emissivity of the black coating being 0.998 [8]. The radiometer operates slightly above 300 K and the solar radiant power entering the cavity is approximately 68 mW, which is estimated from the nominal solar constant of 136 mW/cm^2 and the aperture area of 0.5 cm^2 (0.8 cm diameter).

The selection of the electrical heating method and the temperature sensor location is critical for the measurement accuracy. Three different electrical heating methods are considered in this study. In the first method, the heater wire is wrapped around the cavity from $Z=5$ to 8 mm. In the second method, the heater is located at 1 mm from the end of the cylinder and wrapped in parallel with the inclined end plate with a 3-mm width. In the third method, a thin-film heater is sandwiched between two 12.5-μm-thick Kapton (polyimide) films [9], and then attached to the end plate [5].

The Finite Element Model

The thermophysical properties of the materials are assumed constant because their variations are negligibly small in the room temperature range. The thermophysical properties of the black coating are assumed to be the same as those of nickel, except for the emissivity, because the phosphorous content is very low. For Ag, the thermal conductivity $k=429$ W/m·K, specific heat $c_p=235$ J/kg·K, and density $\rho=10500$ kg/m^3 [10]; for Ni, $k=90.7$ W/m·K, $c_p=444$ J/kg·K, and $\rho=8900$ kg/m^3 [10]; for Kapton, $k=0.12$ W/m·K, $c_p=1090$ J/kg·K, and $\rho=1420$ kg/m^3 [9]. The

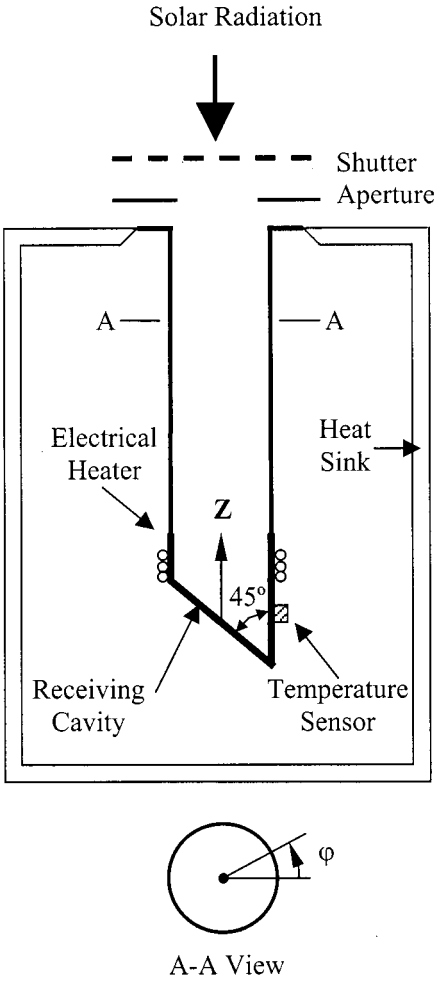

Fig. 1 Schematic of the proposed radiometer for the total solar irradiance measurement

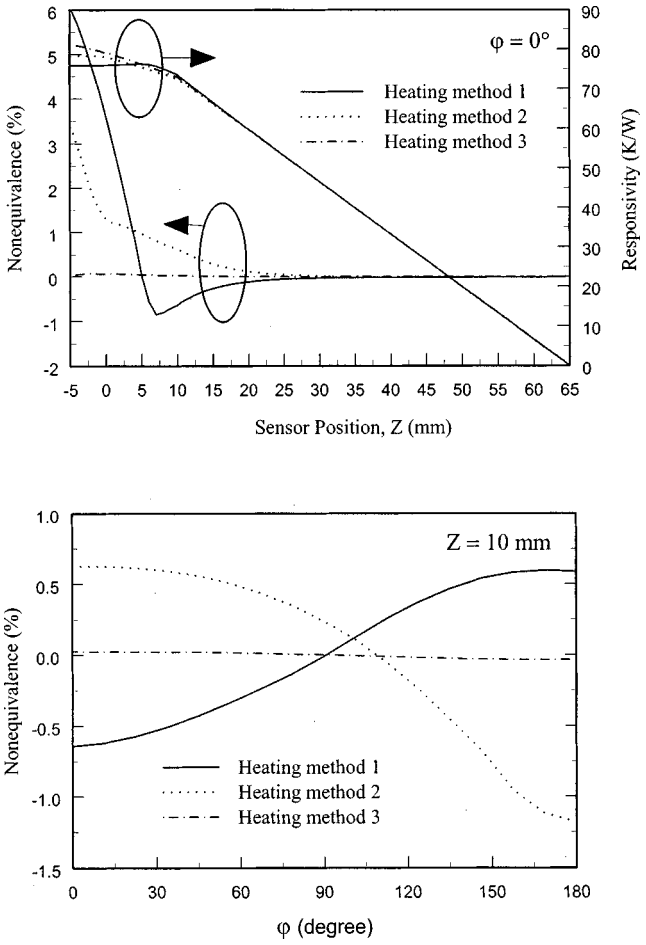

Fig. 2 Responsivity and nonequivalence versus sensor position Z for φ=0° (upper) and nonequivalence versus φ for Z=10 mm (lower)

emissivity of Ag is taken to be 0.02 [10]. The leads of the electrical heater and temperature sensor are omitted since little heat flow passes through them and their heat capacities are small compared to the cavity. The heat capacities of the heating element and temperature sensor are also negligible compared with that of the cavity. Convection is negligible since the radiometer is operated in vacuum. Contact resistances are also neglected. In the present model, however, radiation is considered for both the inside and outside surfaces of the cavity. The actual shutter portion includes a buffer section with its inner walls coated black and maintained at the same temperature as the heat sink. The model treats the aperture as an isothermal black surface. The heat sink is simplified as a constant-temperature surrounding. Radiative heat transfer between the surface elements inside the cavity is calculated using a radiation matrix that includes the view factors and emissivity. Radiative heat loss for the outside surface is calculated using surface effect elements. In the present study, the temperatures of the aperture and heat sink are set to be 312 K. The power is directly applied to the nodes of the heating region. The electrical heating region depends on the heating method. The input of solar radiation is modeled as uniform heating on the end plate.

Four-node tetrahedral elements are used for the end part ($Z<10$ mm) because of the complicated geometry, and six-node prism elements are used for the rest of the cylindrical wall by directly extruding the already meshed part along the axial direction. A total of 7513 solid elements are generated through the automatic meshing procedure. The cross section of the meshed cylindrical wall in the model is not circular, which may yield a slightly smaller cross-sectional area. Corrections could be made by using second-order elements (such as the 20-node hexahedral elements) or by modifying the thickness. This is not done in the present study because the actual thicknesses of the silver and coating may deviate from the design values. A total of 2356 shell elements are used for the black coating that overlaps the inside surface of the silver cavity. A total of 2110 surface elements with negligible thickness are employed for the radiative boundary condition of the outside surface.

The FE analysis employs the Newton-Raphson method to solve the matrix equation, which is nonlinear due to radiation. The results converge to less than 1 nK after three iterations. It takes a few minutes to run a steady-state simulation with a 400 MHz personal computer, after the radiation matrix is solved. The heat flux through the cylindrical cavity for the one-dimensional conduction without considering radiation (by assuming the boundaries are adiabatic) can be obtained analytically by prescribing a uniform temperature for the lower section of the cavity below $Z=10$ mm. The relative difference between the FE analysis and the analytical solution in the simple case is approximately 1.5×10^{-5}. Comparing the FE model with adiabatic boundary conditions to that with radiation boundary conditions for the same input power, the temperature rise near the end of the cavity is

about 2 percent higher in the adiabatic case (when the heat transfer is through conduction only). This suggests that the heat transfer is dominated by conduction.

Results

The calculated responsivity and nonequivalence as functions of the sensor position Z for $\varphi=0$ (see Fig. 1) and the nonequivalence as a function of φ for $Z=10$ mm with different heating methods are shown in Fig. 2. The responsivity is calculated with an 80 mW electrical power input without radiant power. To compute the nonequivalence, the electrical power is set to be 80 mW for the shutter-closed mode and 12 mW for the shutter-open mode with 68 mW radiant power. For all three heating methods, the responsivity increases almost linearly as Z decreases from the opening until $Z\approx20$ mm. Below $Z=10$ mm, the responsivity depends on the heating method. To achieve a responsivity of above 70 K/W, it is desirable to locate the sensor at or below $Z=10$ mm.

The nonequivalence is the smallest near the opening but the responsivity is too low to be acceptable. It can be seen from Fig. 2 that the nonequivalence varies significantly at $Z<10$ mm and is the smallest for heating method 3. The nonequivalence is also a function of φ, and the location near $\varphi=90°$ yields the smallest nonequivalence in all three cases.

A transient analysis for the radiometer cavity is also performed to facilitate the design of a feedback temperature controller. The sensor-temperature history to a step power is calculated and fitted to an exponential curve. The fitting yields in a natural time constant of about 20 s. The single-time-constant exponential function causes a large error at the beginning. Therefore, an improved model, called the two-lumped-heat-capacitance model, has been developed to approximate the transient behavior for use in the optimization of the temperature controller [5].

Conclusion

A three-dimensional FE model has been built for the proposed radiometer cavity and used to calculate its thermal response. The analysis predicts the responsivity, natural time constant, and the nonequivalence between the shutter-closed and shutter-open modes. The optimized location of the temperature sensor can be determined based on the steady-state responsivity and nonequivalence analysis. The FE model developed in this work can easily be extended to other geometries and heating methods to facilitate future design of absolute radiometers.

Acknowledgment

This work was supported by the NIST Optical Technology Division. Steven Lorentz of NIST provided detailed information about the proposed radiometer. Z.M. Zhang acknowledges the support of NSF through a PECASE grant.

References

[1] Fröhlich, C., 1991, ''History of Solar Radiometry and the World Radiometric Reference,'' Metrologia, **28**, pp. 111–115.
[2] Mahan, J. R., Tira, N. E., Lee, III, R. B., and Keynton, R. J., 1989, ''Comparison of the Measured and Predicted Response of the Earth Radiation Budget Experiment Active Cavity Radiometer During Solar Observations,'' Appl. Opt., **28**, pp. 1327–1337.
[3] Hengstberger, F., ed., 1989, *Absolute Radiometry: Electrically Calibrated Thermal Detectors of Optical Radiation*, Academic Press, San Diego, CA, Chap. 1.
[4] Fröhlich, C., and Lean, J., 1998, ''Total Solar Irradiance Variations: The Construction of a Composite and Its Comparison with Models,'' *IAU Symposium 185: New Eyes to See Inside the Sun and Stars*, F. L. Deubner, ed., Kluwer Academic, Dordrecht, The Netherlands, pp. 89–102.
[5] Shen, Y. J., Chen, D. H., and Zhang, Z. M., 1999, ''Thermal Analysis of an Absolute Radiometer Designed for the Future Satellite Mission of Total Solar Irradiance Measurement,'' *1999 International Mechanical Engineering Congress and Exposition*, ASME HTD, 364-4, pp. 189–197.
[6] Gentile, T. R., Houston, J. M., Hardis, J. E., Cromer, C. L., and Parr, A. C., 1996, ''National Institute of Standards and Technology High-Accuracy Cryogenic Radiometer,'' Appl. Opt., **35**, pp. 1056–1068.
[7] Zhang, Z. M., Datla, R. U., Lorentz, S. R., and Tang, H. C., 1994, ''Thermal Modeling of Absolute Cryogenic Radiometers,'' ASME J. Heat Transfer, **116**, pp. 993–998.
[8] Kodama, S., Horiuchi, M., Kunii, T., and Kuroda, K., 1990, ''Ultra-Black Nickel-Phosphorus Alloy Optical Absorber,'' IEEE Trans. Instrum. Meas., **39**, pp. 230–232.
[9] Kapton, polyimide film, E. I. DuPont de Nemours and Company, Wilmington, DE.
[10] Incropera, F. P., and DeWitt, D. P., 1996, *Fundamentals of Heat and Mass Transfer*, 4th Ed., Wiley, New York, Appendix A.